metastatic liver tumor, normal liver parenchyma, kidney, and spleen were excised under anesthesia. The analysis time points were 2, 12, 24, 72, 168, 336, 504, 672, and 1,008 hours after NK012 or CPT-11 administration. Pharmacokinetic analysis was conducted using three mice for each time point. The samples were rinsed sufficiently with 0.9% NaCl solution, mixed with 0.1 mol/L glycine-HCl buffer (pH 3.0)/methanol at 5% (w/w), and then homogenized using Precellys 24 (Bertin Technologies). Free SN-38, NK012, and CPT-11 were extracted from each sample, and the extracted sample was analyzed by reversed-phase high-performance liquid chromatography as described previously (17, 19).

Histopathologic analysis

For conventional histopathologic analysis, the liver with a metastatic tumor was excised from the mice bearing liver metastases as described above. The liver was excised after 15 days from the initiation of each treatment and fixed in buffered 4% paraformaldehyde for 72 hours and embedded in paraffin. Then, 3-μm-thick sections were prepared and stained with H&E.

Biodistribution of NK012 as determined by immunohistochemistry and immunofluorescence microscopy

To evaluate the detailed biodistribution of NK012 in immunohistologic sections, we used 20-nm-sized fixable fluorospheres that have equal diameter to NK012 (FluoSpheres, red fluorescent latex microspheres; Molecular Probes) as a reference of positional relationship within the tissue. Because NK012 could neither be fixed nor stained with other antibodies, we applied this fluorescent-labeled macromolecular substance whose surface is carboxylate modified to decrease nonspecific binding. Five minutes after NK012 administration (30 mg/kg) to mice with liver metastases, fluorospheres (0.25 mL/animal; concentration, 2.5 mg/mL) were also injected i.v. The mice were sacrificed under deep anesthesia and perfused with 0.9% NaCl through the inferior vena cava to prevent blood stasis, and then the liver with metastases was excised 2 hours and 1, 3, and 7 days from the administration of NK012 and fluorospheres. The samples were embedded in an OCT compound (Sakura Finetechnochemical) and quickly frozen in liquid nitrogen.

For direct observation of the fluorescence of NK012 and fluorospheres, 10-μm-thick frozen sections were prepared using a cryostat and examined under a fluorescence microscope (BIOREVO BZ9000; Keyence) at an excitation wavelength of 377 nm and an emission wavelength of 447 nm to evaluate NK012 distribution. For immunohistochemical analysis, frozen sections were prepared as described earlier and fixed in 4% paraformaldehyde in PBS (pH 7.4). After blocking, sections were incubated for 1 hour at room temperature with primary antibodies. Anti-CD31 goat antibody for endothelial cells (R&D Systems) was used at 1:200 dilution, and anti-CD68 rat antibody for macrophages (Kupffer cells; AbD Serotec) was used at 1:200 dilution. The sections were then incubated with the following secondary antibodies at 1:500 dilution: Alexa 647 donkey anti-goat IgG, Alexa 488 goat anti-rat IgG, or Alexa 647 goat anti-rat IgG. Nuclei were

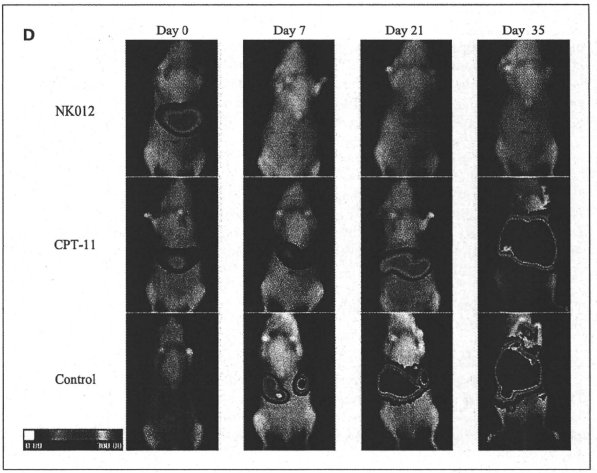

Fig. 1. ***Continued.*** D, images of an HT-29/Luc mouse model treated with each regimen taken using a Photon Imager system on days 0, 7, 21, and 35 after therapy initiation. Points, mean; bars, SD. Arrows, drug injections. Statistical comparisons between the NK012 group and the CPT-11 group were done by ANOVA on day 28 after treatment initiation ($P < 0.0001$).

counterstained with 4′,6-diamidino-2-phenylindole at 1:1,000 dilution (Roche).

Statistical analysis

Data were expressed as mean ± SD. To evaluate changes in the photon count of each treatment group, repeated-measures ANOVA was used. Survival was assessed using the Kaplan-Meier method. For all tests, P values of <0.05 were considered significant using SPSS software version 12.0 (SPSS, Inc.). All statistical tests were two-sided.

Results

Antitumor activity of NK012 and CPT-11 against HT-29/Luc liver metastasis model

Comparison of the relative photon count on day 28 in the HT-29/Luc liver metastasis model revealed significant differences between mice given NK012 and those given CPT-11 ($P = 0.002$; Fig. 1A, B, and D). The survival rates on day 140 in the three test groups were 100%, 0%, and 0% for the NK012, CPT-11, and control groups, respectively (Fig. 2). Moreover, neither relapse nor any other clinical problems were observed in the NK012 group until day 140. Kaplan-Meier analysis showed that a significant improvement in the survival rate was observed in the NK012 group compared with the CPT-11 group ($P = 0.0006$), whereas there was no significant improvement between the CPT-11 group and the control group ($P = 0.1556$). There was no severe body weight loss or toxic death for any treatment used in this study (Fig. 1C).

Histopathologic findings

Histopathologic observation of liver metastases after NK012 administration showed the disappearance of tumor cells. Tumor tissue was replaced with fibrotic or granulomatous tissue with mild infiltration of inflammatory cells. On the other hand, liver metastases treated with CPT-11 showed slight degeneration of cancer cells and few apoptotic cells (Fig. 3). At the liver parenchyma, sinusoidal dilation or steatosis that was a characteristic feature of chemotherapy-associated liver toxicity was not observed after a single or triple administration of NK012.

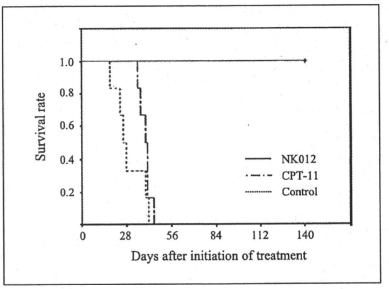

Fig. 2. Kaplan-Meier curves of HT-29/Luc liver metastasis models. The NK012 group (30 mg/kg/d), CPT-11 group (66.7 mg/kg/d), and control group (PBS, 200 μL/d) were administered each drug on days 0, 4, and 8 ($n = 6$). Treatment was initiated 7 d after the portal injection of HT-29/Luc cells. Log-rank test: NK012 group versus CPT-11 group, $P = 0.0006$; CPT-11 group versus control group, $P = 0.1556$.

Tissue concentration and transition of SN-38 after NK012 and CPT-11 administration

We investigated the concentration-time profile of NK012, CPT-11, and free SN-38 in various tissues after single i.v. administration more precisely compared with a previous report (17). The accumulation of free SN-38 converted from CPT-11 was rapidly decreased within 24 hours and could not be detected thereafter in the plasma (Fig. 4A), liver, spleen, kidney, and liver tumor (Fig. 4B). In contrast, the accumulation of free SN-38 released by NK012 was maintained at a relatively high level for weeks after administration. Notably, prolonged higher accumulation of free SN-38 and NK012 was observed in the liver and spleen, which are organs categorized under the reticuloendothelial system. The concentrations of free SN-38 and NK012 gradually decreased over 6 weeks.

Biodistribution of NK012 in hepatic metastases and liver parenchyma

First, we observed directly the distribution and relationship of NK012 and fluorospheres to confirm the detailed biodistribution of NK012 in tissue. In the metastatic tumor, the biodistribution of both substances was similar after 24 hours following their administration, whereas a discrepancy was found at 2 hours (Fig. 5A). For the normal liver parenchyma, fluorescence microscopy showed a similar biodistribution of NK012 and fluorospheres with the exception of the weak accumulation of NK012 2 hours after administration (Fig. 5B).

Second, we observed fluorospheres as a reference of NK012 distribution by immunohistochemistry. Anti-CD31 and anti-CD68 antibodies were used as vascular endothelial cell and macrophage (Kupffer) cell markers, respectively. Fluorospheres distributed around tumor vessels in the metastatic liver tumor in all observation points (Fig. 6A). For the liver parenchyma, fluorospheres were not observed in the hepatocytes but were well phagocytized by CD68-positive Kupffer cells in all observation points (Fig. 6B). In addition, the number of CD68-positive cells did not decrease significantly (data not shown).

Discussion

This study highlights four novel findings. First, NK012 was strongly effective in mice bearing liver metastases of human colorectal cancer cells. Second, free SN-38 released from NK012 showed high accumulation and NK012 was detected in the liver metastatic tumor for a long time. Third, free SN-38 and NK012 had been retained in the liver and spleen for weeks with no accompanying toxicity to normal

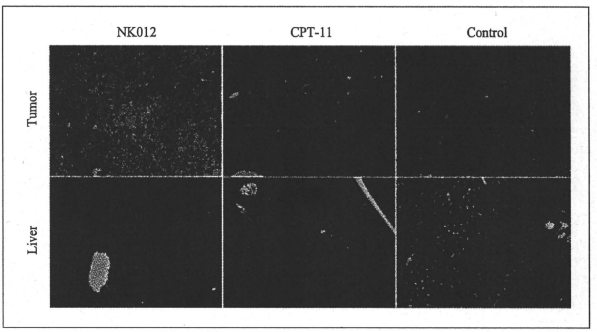

Fig. 3. H&E-stained sections of metastatic tumor and liver treated with NK012 and CPT-11. Scale bars, 100 μm. NK012 (30 mg/kg/d), CPT-11 (66.7 mg/kg/d), and PBS (200 μL/d) were administered on days 0, 4, and 8 following the same schedule as the treatment studies. Metastatic tumors and livers were excised on day 15 after treatment initiation.

organs either symptomatically or pathologically. Fourth, NK012 entrapment by macrophages in the liver and spleen led to its prolonged accumulation, and NK012 retention around tumor vessels also resulted in its relatively high accumulation lasting for weeks.

To our knowledge, this is the first study to show that NK012 completely eradicated orthotopic tumors in an orthotopic model, in addition to our previously reported potent antitumor effects of NK012 against various models using human cancer cell lines (17–20, 25). The strong antitumor activity of NK012 is attributable to the high concentration of free SN-38 released from NK012 in the tumor, which is higher than any other concentrations previously reported. Liver metastasis in a specific organ has an adequate potential to be a target of DDS agents, although it presents a disadvantage for such agents because it is considered a hypovascular tumor.

The accumulation and metabolism of DDS agents are closely associated with their biodistribution. The two major differences about the distribution between NK012 and fluorospheres 2 hours after administration in direct fluorescence observation are the lower accumulation of NK012 in the liver parenchyma and discrepancy in metastatic liver tumor (Fig. 5A and B). In agreement with previous reports, these data indicate that NK012 extravasation was successfully achieved and NK012 uptake by Kupffer cells was less than fluorosphere uptake during the early phase after administration because of the higher biocompatibility of the outer shell, which was enveloped by polyethyleneglycol (26–28). NK012 biodistribution was similar to fluorosphere biodistribution after 24 hours following administration, and therefore, this fixable fluorescence-labeled nanoparticle can be considered as a substitute for NK012 observation in histochemical studies after such period. Considering these facts, NK012 was retained around CD31-positive tumor vessels in the metastatic tumors and stored in CD68-positive macrophage cells in the liver parenchyma during the late phase after administration, thereby resulting in the high concentration of free SN-38 in the tumor and liver for weeks.

The metabolic pathway of NK012 also plays an important role in organ toxicities. Specifically, the mechanism of liver injury has not yet been clarified, but it is speculated that mitochondrial damage due to cytotoxic agents and the resulting reactive oxygen species have some effect on liver toxicities (29). As for NK012 and CPT-11, SN-38 is detoxified mainly in normal liver cells to form SN-38 β-glucuronide (inactive form) by UDP-glucuronosyltransferase, and the detoxification capability may be related to liver toxicities (30). In this study, the single or triple administration of NK012 at the maximum tolerable dose showed no chemotherapy-associated liver toxicity in terms of pathologic changes (Fig. 3) and blood biochemical findings, which reflects hepatocyte injury (data not shown). Daemen et al. (31) reported severe depletion of liver macrophages 24 hours after the administration of liposomal doxorubicin and emphasized the possibility of developing infection due to depletion of the phagocytic capacity of the reticuloendothelial system. Notably, our present data are not in agreement with those of Daemen et al. The number of CD68-positive cells did not decrease because NK012, which is endocytosed in Kupffer cells, is rapidly transported to an acidic environment (pH <5.0), and this novel polymeric micelle agent is very stable at such an acidic condition, indicating that NK012 gradually releases free SN-38 after it accumulates in Kupffer cells (17, 32). Given the metabolite pathway of SN-38 and present data, NK012 causes neither injury of hepatocytes nor depletion of Kupffer cells. However, further studies of liver toxicity with repeated NK012 administrations and the detoxification capability of SN-38, which is gradually released from NK012 for a long period, are needed to clarify whether the prolonged use of NK012 causes chemotherapy-associated liver toxicity or not.

A limitation of this study is the difficulty in the observation of NK012 or free SN-38 by fluorescence microscopy to show their detailed biodistribution. This is because

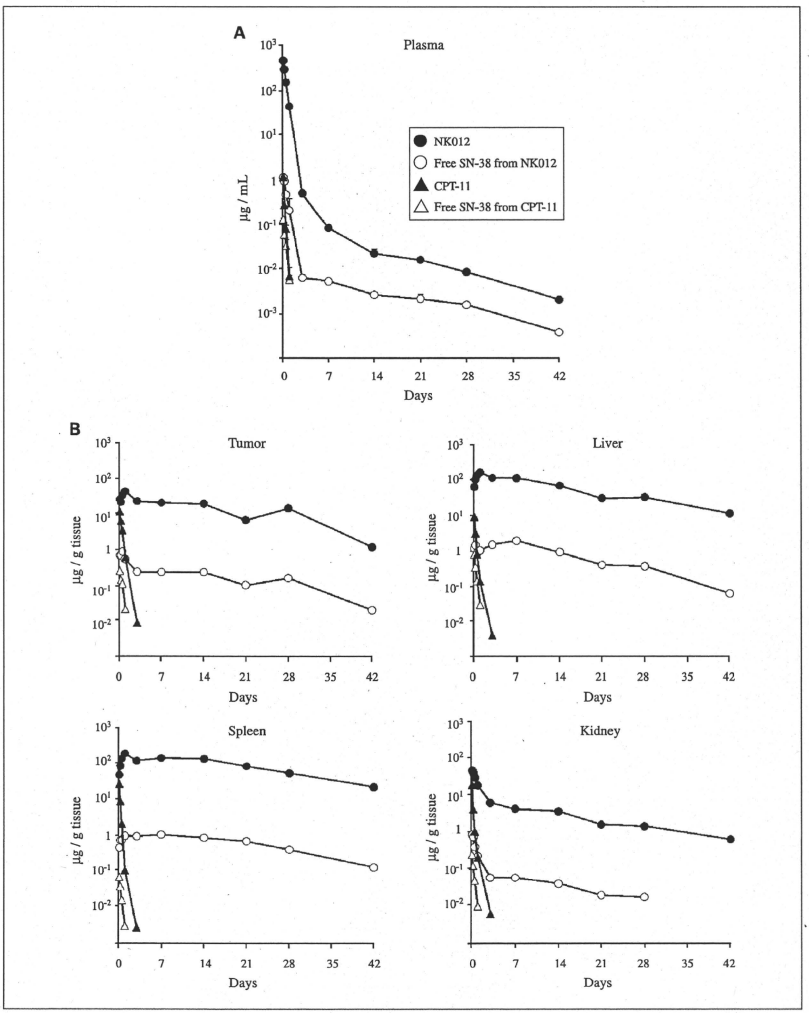

Fig. 4. Transition of plasma and tissue concentration after single administration of NK012 (30 mg/kg) or CPT-11 (66.7 mg/kg) to HT-29/Luc liver metastasis mouse models (n = 3). A, plasma. B, tissue. ●, NK012; ○, free SN-38 released from NK012; ▲, CPT-11; △, free SN-38 converted from CPT-11. Points, mean; bars, SD. Arrows, drug injections.

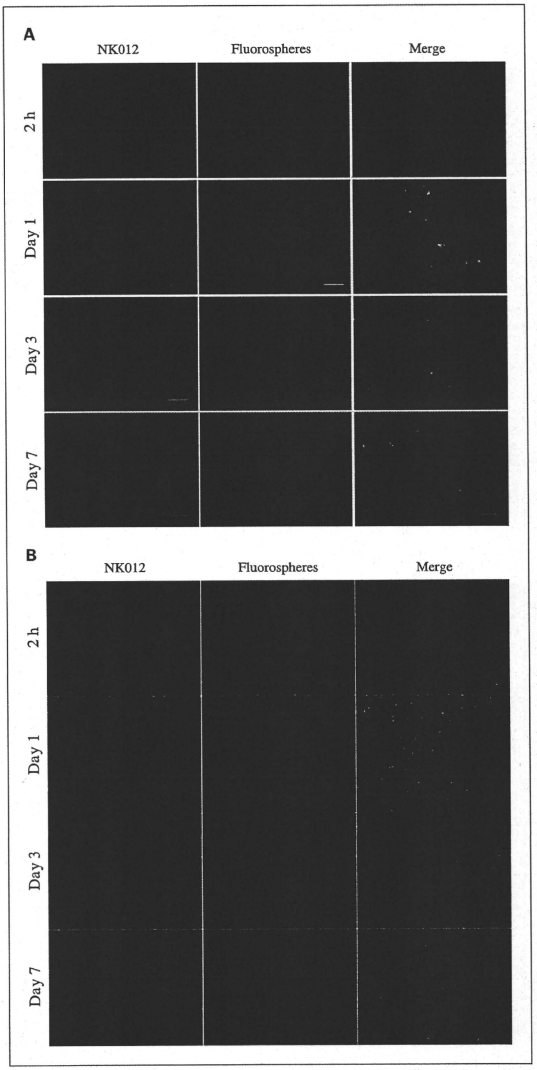

Fig. 5. Biodistribution of NK012 and fluorospheres in hepatic metastasis and liver parenchyma for assessment of distributional relationship of the two substances. Frozen sections of livers from HT-29/Luc liver metastasis nude mice administered NK012 and fluorospheres were directly observed by fluorescence microscopy. A, liver metastatic tumor. Scale bars, 50 μm. B, liver parenchyma. Scale bars, 100 μm.

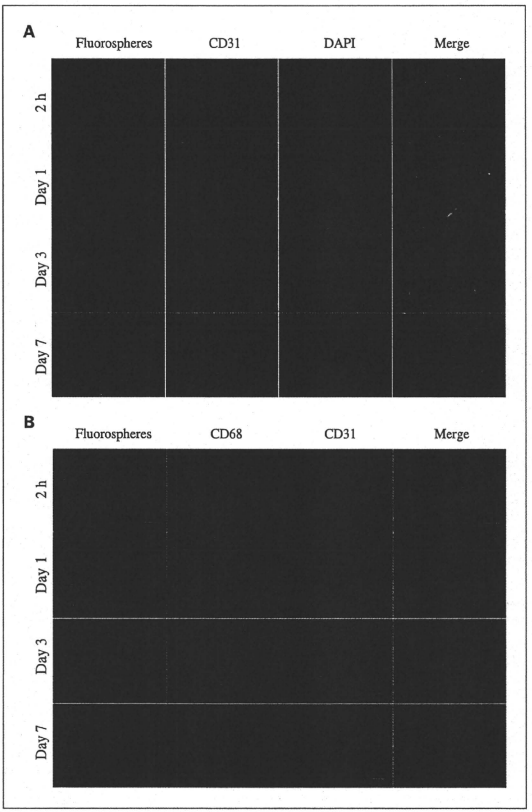

Fig. 6. Immunohistochemical analysis to assess fluorosphere distribution as criteria of NK012 biodistribution. Frozen sections of livers from HT-29/Luc liver metastasis nude mice administered NK012 and fluorospheres were stained immunohistochemically followed by fluorescence microscopy observations. A, liver metastatic tumor. Scale bars, 50 μm. B, liver parenchyma. Scale bars, 100 μm.

NK012 cannot be fixed and the fluorescence intensities of NK012 and free SN-38 are very weak. Here, we used 20-nm-sized fixable fluorospheres as a substitute for NK012, although direct observation of the object substance remains the best method to verify NK012 biodistribution. There is, however, a technical difficulty in developing a fixable fluorescence substance with entirely the same properties as those of developed DDS agents.

CPT-11 has been approved for the treatment of advanced colorectal cancer in combination with other agents such as fluorouracil, leucovorin, and molecular targeting agents. However, the intensive use of CPT-11 induces chemotherapy-associated steatohepatitis, which affects mortality or morbidity of hepatectomy. NK012 is a biocompatible agent for the treatment of CLM and an excellent SN-38 vehicle because SN-38 is a time-dependent anticancer agent, and the appropriate SN-38 concentration released by NK012 is well maintained for a long time in liver metastases. In terms of liver toxicity, NK012 seems to be nontoxic as shown in this study regardless of the long-term storage of NK012 in Kupffer cells.

In conclusion, NK012 showed strong antitumor effects against liver metastatic tumor. NK012 well infiltrates metastatic tumor tissue and cannot be easily endocytosed by

macrophages during the early phase after administration. The excellent biodistribution and metabolite pathway of NK012 corroborates both its strong antitumor effects and low toxicity. Our data warrant clinical evaluation of NK012 for the treatment of liver metastases of colorectal cancer.

Disclosure of Potential Conflicts of Interest

No potential conflicts of interest were disclosed.

Acknowledgments

A. Takahashi would like to thank the Foundation for Promotion of Cancer Research (Japan) for the Third-Term Comprehensive Control Research for Cancer for awarding him a research resident fellowship. We thank N. Mie and M. Ohtsu for technical assistance and K. Shiina and K. Abe for secretarial assistance.

Grant Support

Grant-in-Aid for Third-Term Comprehensive Control Research for Cancer from the Ministry of Health, Labour and Welfare of Japan (Y. Matsumura); Scientific Research on Priority Areas grant 17016087 from the Ministry of Education, Culture, Sports, Science and Technology (Y. Matsumura); Japanese Foundation for Multidisciplinary Treatment of Cancer (Y. Matsumura); and Princess Takamatsu Cancer Research Fund grant 07-23908.

The costs of publication of this article were defrayed in part by the payment of page charges. This article must therefore be hereby marked *advertisement* in accordance with 18 U.S.C. Section 1734 solely to indicate this fact.

Received 05/31/2010; revised 08/15/2010; accepted 08/18/2010.

References

1. Scheele J, Stang R, Altendorf-Hofmann A, Paul M. Resection of colorectal liver metastases. World J Surg 1995;19:59–71.
2. Steele G, Jr., Ravikumar TS. Resection of hepatic metastases from colorectal cancer. Biologic perspective. Ann Surg 1989;210:127–38.
3. Bismuth H, Adam R, Levi F, et al. Resection of nonresectable liver metastases from colorectal cancer after neoadjuvant chemotherapy. Ann Surg 1996;224:509–20.
4. Adam R, Delvart V, Pascal G, et al. Rescue surgery for unresectable colorectal liver metastases downstaged by chemotherapy: a model to predict long-term survival. Ann Surg 2004;240:644–57.
5. Hurwitz H, Fehrenbacher L, Novotny W, et al. Bevacizumab plus irinotecan, fluorouracil, and leucovorin for metastatic colorectal cancer. N Engl J Med 2004;350:2335–42.
6. Diaz-Rubio E, Tabernero J, Gomez-Espana A, et al. Phase III study of capecitabine plus oxaliplatin compared with continuous-infusion fluorouracil plus oxaliplatin as first-line therapy in metastatic colorectal cancer: final report of the Spanish Cooperative Group for the Treatment of Digestive Tumors Trial. J Clin Oncol 2007;25:4224–30.
7. Fernandez FG, Ritter J, Goodwin JW, Linehan DC, Hawkins WG, Strasberg SM. Effect of steatohepatitis associated with irinotecan or oxaliplatin pretreatment on resectability of hepatic colorectal metastases. J Am Coll Surg 2005;200:845–53.
8. Rubbia-Brandt L, Audard V, Sartoretti P, et al. Severe hepatic sinusoidal obstruction associated with oxaliplatin-based chemotherapy in patients with metastatic colorectal cancer. Ann Oncol 2004;15:460–6.
9. Karoui M, Penna C, Amin-Hashem M, et al. Influence of preoperative chemotherapy on the risk of major hepatectomy for colorectal liver metastases. Ann Surg 2006;243:1–7.
10. Aloia T, Sebagh M, Plasse M, et al. Liver histology and surgical outcomes after preoperative chemotherapy with fluorouracil plus oxaliplatin in colorectal cancer liver metastases. J Clin Oncol 2006; 24:4983–90.
11. Kopetz S, Hoff PM, Morris JS, et al. Phase II trial of infusional fluorouracil, irinotecan, and bevacizumab for metastatic colorectal cancer: efficacy and circulating angiogenic biomarkers associated with therapeutic resistance. J Clin Oncol 28:453–9.
12. Reddy SK, Morse MA, Hurwitz HI, et al. Addition of bevacizumab to irinotecan- and oxaliplatin-based preoperative chemotherapy regimens does not increase morbidity after resection of colorectal liver metastases. J Am Coll Surg 2008;206:96–106.
13. Mathijssen RH, van Alphen RJ, Verweij J, et al. Clinical pharmacokinetics and metabolism of irinotecan (CPT-11). Clin Cancer Res 2001; 7:2182–94.
14. Slatter JG, Schaaf LJ, Sams JP, et al. Pharmacokinetics, metabolism, and excretion of irinotecan (CPT-11) following I.V. infusion of [14C] CPT-11 in cancer patients. Drug Metab Dispos 2000;28:423–33.
15. Rothenberg ML, Kuhn JG, Burris HA III, et al. Phase I and pharmacokinetic trial of weekly CPT-11. J Clin Oncol 1993;11:2194–204.
16. Matsumura Y, Maeda H. A new concept for macromolecular therapeutics in cancer chemotherapy: mechanism of tumoritropic accumulation of proteins and the antitumor agent smancs. Cancer Res 1986;46:6387–92.
17. Koizumi F, Kitagawa M, Negishi T, et al. Novel SN-38-incorporating polymeric micelles, NK012, eradicate vascular endothelial growth factor-secreting bulky tumors. Cancer Res 2006;66:10048–56.
18. Sumitomo M, Koizumi F, Asano T, et al. Novel SN-38-incorporated polymeric micelle, NK012, strongly suppresses renal cancer progression. Cancer Res 2008;68:1631–5.
19. Kuroda J, Kuratsu J, Yasunaga M, Koga Y, Saito Y, Matsumura Y. Potent antitumor effect of SN-38-incorporating polymeric micelle, NK012, against malignant glioma. Int J Cancer 2009;124:2505–11.
20. Nakajima TE, Yanagihara K, Takigahira M, et al. Antitumor effect of SN-38-releasing polymeric micelles, NK012, on spontaneous peritoneal metastases from orthotopic gastric cancer in mice compared with irinotecan. Cancer Res 2008;68:9318–22.
21. Alexis F, Pridgen E, Molnar LK, Farokhzad OC. Factors affecting the clearance and biodistribution of polymeric nanoparticles. Mol Pharmacol 2008;5:505–15.
22. Lee MJ, Veiseh O, Bhattarai N, et al. Rapid pharmacokinetic and biodistribution studies using cholorotoxin-conjugated iron oxide nanoparticles: a novel non-radioactive method. PLoS One 5:e9536.
23. Peer D, Karp JM, Hong S, Farokhzad OC, Margalit R, Langer R. Nanocarriers as an emerging platform for cancer therapy. Nat Nanotechnol 2007;2:751–60.
24. Zamboni WC. Liposomal, nanoparticle, and conjugated formulations of anticancer agents. Clin Cancer Res 2005;11:8230–4.
25. Kuroda J, Kuratsu J, Yasunaga M, et al. Antitumor effect of NK012, a 7-ethyl-10-hydroxycamptothecin-incorporating polymeric micelle, on U87MG orthotopic glioblastoma in mice compared with irinotecan hydrochloride in combination with bevacizumab. Clin Cancer Res 16:521–9.
26. Allen TM, Cullis PR. Drug delivery systems: entering the mainstream. Science 2004;303:1818–22.
27. Duncan R. The dawning era of polymer therapeutics. Nat Rev Drug Discov 2003;2:347–60.
28. Gabizon AA. Stealth liposomes and tumor targeting: one step further in the quest for the magic bullet. Clin Cancer Res 2001;7:223–5.
29. Chun YS, Laurent A, Maru D, Vauthey JN. Management of chemotherapy-associated hepatotoxicity in colorectal liver metastases. Lancet Oncol 2009;10:278–86.
30. Rouits E, Charasson V, Petain A, et al. Pharmacokinetic and pharmacogenetic determinants of the activity and toxicity of irinotecan in metastatic colorectal cancer patients. Br J Cancer 2008;99:1239–45.
31. Daemen T, Hofstede G, Ten Kate MT, Bakker-Woudenberg IA, Scherphof GL. Liposomal doxorubicin-induced toxicity: depletion and impairment of phagocytic activity of liver macrophages. Int J Cancer 1995;61:716–21.
32. Schreiber R, Zhang F, Haussinger D. Regulation of vesicular pH in liver macrophages and parenchymal cells by ammonia and anisotonicity as assessed by fluorescein isothiocyanate-dextran fluorescence. Biochem J 1996;315:385–92.

RESEARCH ARTICLE

SPECIAL FOCUS: ONCOLOGY

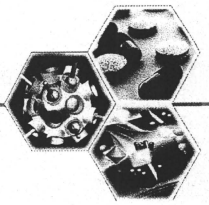

Optimum conditions of ultrasound-mediated destruction of bubble liposome for siRNA transfer in bladder cancer

Background: We investigated the effectiveness of ultrasound-mediated destruction of bubble liposome (UBL) for siRNA transfer by observing reduction in the luciferase activity of human bladder tumor RT-112 cells transfected with the luciferase gene (*RT-112Luc*) following luciferase siRNA transfer into the cells. **Results:** siRNA was transferred to 26% of RT-112Luc cells by UBL and the luciferase activity of RT-112Luc cells was significantly suppressed by UBL using the luciferase siRNA, compared with that using nonspecific siRNA *in vitro* ($p = 0.036$). The luciferase activity of RT-112Luc tumor was suppressed by UBL using luciferase siRNA compared with that using nonspecific siRNA 2 days after the *in vivo* treatment. **Conclusion:** This study showed that UBL is suitable for siRNA transfer to mammalian cells.

Bladder cancer is classified into two types, superficial and invasive. In clinics, 70% of bladder cancers are reported to be the superficial type, which does not invade the muscle layer of the bladder wall [1]. The standard treatment of superficial bladder cancers is transurethral resection of the bladder cancer followed by the intravesical instillation of an anticancer drug or Bacillus Calmette–Guerin (BCG) to prevent tumor recurrence.

However, in half of surgically treated patients, bladder tumors recur and 10–30% of recurrent bladder tumors become invasive. Patients with an invasive tumor inevitably undergo radical cystectomy. Moreover, subsidiary BCG treatment usually causes unbearable cystitis manifested with fever and local pain [2]. Therefore, a new modality that results in good quality of life and prevents the recurrence of the superficial bladder tumor is urgently needed.

siRNA is a sequence-specific double-strand RNA and has been newly recognized as a powerful and useful tool for gene expression inhibition [3,4]. The RNAi effect on the cytosol is transient and the 'off or on' of the treatment can be readily controlled [5]. When side effects induced by RNAi occur, treatment can be stopped before the occurrence of serious side effects. As sequence-specific siRNA can be prepared exquisitely using sequence information, RNAi therapy may have the possibility to be a new, convenient and safe modality in clinics. Recently, the intravesical application of RNAi targeting PLK-1 in a mice bladder cancer model using cationic liposome has been reported as a new therapy for bladder cancer [6]. Furthermore, plasmid DNA transfection [7–13] and siRNA [13–18] to cells using sonoporation, combined with ultrasound (US) and microbubble has been reported. Microbubble has been demonstrated to collapse by US irradiation; transient permeability of the cell membrane occurred by the cavitation following the destruction of microbubble and finally the plasmid DNA was transfected to the cells efficiently [19–21].

Previously, we developed a novel liposomal bubble (bubble liposome [BL]) that encapsulated the perfluoropropane nanobubble in the lipid bilayer [22]. The mean size of the BLs was approximately 800–900 nm, which is smaller than microbubbles used for ultrasound imaging such as Sonazoid™, Optison™ and SonoVue® [23,24]. BLs may be useful for local or systemic delivery of a gene to the target site (cancer tissue) followed by ultrasound exposure to the site for transferring the gene to cancer cells [25].

In this context, we have investigated a new method of siRNA transfection *in vitro* and *in vivo* using ultrasound-mediated destruction of BL.

Experimental

■ Cell line

The human bladder tumor cell line RT-112 was purchased from the American Type Culture Collection (VA, USA). For the *in vitro* experiments and *in vivo* bioluminescence imaging of

Suguru Fujisawa[1,4], Hiroshige Arakawa[1,4], Ryo Suzuki[2], Kazuo Maruyama[2], Tetsuya Kodama[3], Masahiro Yasunaga[4], Yoshikatsu Koga[4] & Yasuhiro Matsumura[†4]

[1]Graduate School of Frontier Science, The University of Tokyo, Japan
[2]School of Pharmaceutical Sciences, Teikyo University, Japan
[3]Graduate School of Biomedical Engineering, Tohoku University, Japan
[4]Investigative Treatment Division, Research Center for Innovative Oncology, National Cancer Center Hospital East, 6–5–1 Kashiwanoha, Kashiwa-City, Chiba 277–8577, Japan
[†]Author for correspondence:
Tel.: +81 4 7134 6857
Fax: +81 4 7134 6866
E-mail: yhmatsum@east.ncc.go.jp

FUTURE SCIENCE part of fsg

subcutaneous tumors, the RT-112 cell line stably expressing firefly luciferase and the YFP mutant Venus RT-112^{Luc} was established. In brief, the coding sequence for firefly luciferase and Venus was subcloned into the pIRES Vector (Clontech Laboratories, CA, USA). The fragment consists of Luciferase-IRES-Venus generated from the plasmid with the restriction enzymes NheI and NotI. This fragment was subcloned into the pEF6/V5-His Vector (Invitrogen, CA, USA) to generate plasmids of pEF6-Luciferase IRES Venus. RT-112 cells were seeded onto 1/6-well plate, 24 h before the transfection. The cells were transfected with pEF6-Luciferase IRES Venus (2 µg) using FuGENE HD transfection reagent (Roche Diagnostics, Mannheim, Germany) according to manufacturer's instructions, and then incubated for 48 h at 37°C. The cells were then passaged in medium containing Blasticidin (10 µg/ml; InvivoGen, CA, USA) to select for the blasticidin-resistance gene integrated in the pEF6/V5-His plasmids. Venus expression was used as a surrogate marker of luciferase-positive RT-112^{Luc}. RT-112^{Luc} cells were sorted using the BD FACS Aria cell sorter (BD Biosciences, CA, USA) and expanded in selection medium. RT-112 and RT-112^{Luc} were grown in Dulbecco's Modified Eagle's Medium (Wako, Tokyo, Japan) containing 10% fetal bovine serum (Tissue Culture Biologicals, CA, USA), 2 mM L-glutamine (Sigma-Aldrich, MO, USA), 100 U/ml penicillin, 100 µg/ml streptomycin and 0.25 µg/ml amphotericin B (100 × antibiotic–antimycotic, GIBCO, CA, USA) in a humidified atmosphere at 37°C and 5% CO_2.

■ US irradiation

The intensity of the US probe (BFC applications, Fujisawa, Japan) used in this study was calibrated using a hydrophone (ONDA, CA, USA) in a water bath. The probe was immersed in the water bath at 0.5 cm from the water surface. The cells were plated in a cell culture plate and mice were immersed in water and irradiated using US.

■ Bubble liposome

Liposomes composed of 1,2-distearoyl-sn-glycero-3-phosphocholine (DSPC, NOF corporation, Tokyo, Japan) and *N*-(carbonyl-methoxypolyethyleneglycol 2000)-1,2-distearoyl-sn-glycero-3-phosphoethanolamine (DSPE-PEG(2k)-OMe, NOF corporation) (94:6 m/m) were prepared by reverse-phase evaporation. In brief, all reagents were dissolved in 1:1 (v/v) chloroform/diisopropyl ether and then 4 ml of phosphate buffered saline (PBS, Invitrogen) was added. The mixture was sonicated and evaporated at 65°C. The solvent was completely removed, and the size of the liposomes was adjusted to less than 200 nm using an extruding apparatus (Northern Lipids Inc., BC, Canada) and sizing filters (pore sizes: 100 and 200 nm; Nuclepore Track-Etch Membrane, Whatman PLC, UK). After sizing, the liposomes were sterilized by passing them through a 0.45-µm pore size filter (MILLEX HV filter unit, Durapore PVDF membrane, Millipore Corporation, MA, USA). BLs were prepared from the liposomes and perfluoropropane gas (Suganuma Sangyo, Tokyo, Japan) [23,26,27]. In brief, 2 ml of 1 mg/ml liposome in PBS was poured into a 5-ml vial (As One, Osaka, Japan). The vial was tightly covered, followed by the addition of 7.5 ml of perfluoropropane gas. To prepare BLs, the vial was shaken vigorously for a few minutes in the Ultra sonic cleaner vs-100 (As One). Being unstable, the BL should be used within 10 min (data not shown).

■ Optimum conditions of UBL *in vitro*

To determine the optimum conditions of UBL, fluorescein isothiocyanate (FITC)-dextran internalization was analyzed by flow cytometry using FACS Calibur (BD Biosciences). RT-112 cells (6.0×10^5) and 500 nM (final concentration) 10 kDa FITC-dextran (Invitrogen) were mixed in flat-bottomed 48-well cell-culture plates (NY, USA) and treated using several conditions of UBL. The US and BL conditions used in this simulation study were as follows; US intensity: 1, 2, 3 or 4 W/cm^2; duration of US irradiation: 10, 30 or 50 s; final concentration of the BL: 0.1, 0.2 or 0.3 mg/ml; interval time of US irradiation after addition of the BL: 15, 30, 60 or 300 s.

At 24 h after the treatment, surviving cells were trypsinized and resuspended in PBS containing 0.5% bovine serum albumin and 2 mM EDTA and FITC-positive cells were analyzed by flow cytometry. FITC-positive cells were defined by comparison of the cells without the treatment as negative control in the gating area of living cells (propidium iodide exclusion method) using flow cytometry.

Cytotoxic effect was also analyzed under the several conditions of UBL. RT-112 cells were treated using the same conditions as described

above. Cell viability was measured by the tetrazolium salt-based proliferation assay (WST assay; Wako Chemicals, Osaka, Japan). Briefly, treated cells (5×10^4 cells/well) in 96-well plates (Corning) were incubated overnight. After incubation for 24 h, the medium was changed to a new medium containing 10% WST-8 reagents. After incubation for 1 h, the absorbance of the formazan product formed was detected at 450 nm in a 96-well spectrophotometric plate reader (SpectraMax 190; Molecular Devices, Sunnyvale, CA, USA). Cell viability was measured and compared with that of the nontreated control cells. *In vitro* tests were conducted in triplicate.

■ Luciferase activity assay *in vitro*

Luciferase activity was analyzed using the Pica Gene luciferase assay system (Toyo Ink, Tokyo, Japan). Cells were harvested by centrifugation at 2000 rpm for 5 min at 4°C and lyzed by the addition of 5 µl of the lysis buffer. The lysate was freezed–thawed in liquid nitrogen. Thereafter, the luciferase activity of 5 ng of protein was quantified.

■ siRNA

The sequence data of siRNA targeted to the luciferase gene and nonspecific siRNA are as follows: luciferase siRNA: 5′-sense strand, 5′-ACAUCACUU ACGCUGAGUACUUCGAAG-3′ and 5′-antisense strand, 5′-UCGAAGUACUCAGCGUAAGUGAUGUAU-3′ (Hokkaido System Science, Sapporo, Japan); nonspecific siRNA: 5′-sense strand, 5′-CCCUCUAGUCUAGCGAGAUAAUUCAAG-3′ and 5′-antisense strand, 5′-UGAAUUAUCUCGCUAGACUAGAGGGAU-3′ (iGENE, Tokyo, Japan). The siRNA was diluted to 100 pmol/µl (µM) by DNase, RNase-free water (GIBCO).

■ siRNA transfection using the optimum conditions of UBL *in vitro* & *in vivo*

siRNA transfection was conducted using the optimum conditions according to the simulation experiment described earlier. RT-112^{Luc} cells (6.0×10^5), siRNA (500 nM, final concentration) and the BL (0.2 mg/ml, final concentration) were plated into a 48-well plate. Then the well was irradiated by US at 1 W/cm^2 for 10 s at 30 s after the addition of the BL. These conditions demonstrated the best transfection efficiency under the condition that more than 60% of cells compared with the nontreated control survive.

■ *In vivo* UBL

RT-112^{Luc} cells (5×10^6 cells/100 µl) were injected subcutaneously in the left back skin of 6-week-old female BALB-c nu/nu mice (SLC, Shizuoka, Japan) (day -5). At 3 and 5 days after tumor implantation (day -2, 0), luciferase activity was measured as count per minute (cpm) using Photon Imager (Biospace, Paris, France). Mice bearing an RT-112^{Luc} tumor (tumor size: 5 mm) were divided into groups consisting of four mice and were treated using UBL and luciferase siRNA or nonspecific siRNA. The mice were then anesthetized with 2,2,2-tribromoethanol (250 mg/kg; Wako) and 2-methyl-2-butanol (250 µl/kg; Wako). Luciferase siRNA (600 pmol) in 80 µl of PBS and 20 µl of the BL were mixed and immediately injected into the tumor. A total of 30 s after intratumor injection of the mixture of the BL and siRNA, the mice were exposed to US irradiation (intensity: 1 W/cm^2, Duty Ratio: 50%, exposure time: 10 s). Intratumor administration of nonspecific siRNA was performed in the same manner as that for the control. After the treatment, luciferase activity was measured as cpm using Photon Imager® until 3 days after the treatment.

All animal procedures were performed in compliance with the Guidelines for the Care and Use of Experimental Animals of the National Cancer Center, Japan; these guidelines meet the ethical standards required by law and also comply with the guidelines for the use of experimental animals in Japan.

■ Histological toxicity of UBL *in vivo*

The PBS (80 µl) and BL (20 µl) were mixed and immediately injected into the left back skin of 6-week-old female BALB-c nu/nu mice. After 30 s from the injection of the BL, these mice were exposed to US irradiation (intensity: 0, 1, 2, 3 or 4 W/cm^2, duty ratio: 50%, exposure time: 10 s). These treatments were conducted three times (days 0, 2 AND 4). Skin lesions were collected 24 h after the last US irradiation and fixed in 3.7% formaldehyde/PBS. Paraffin-embedded tissue was cut (3 µm thick) and deparaffinized, followed by staining with hematoxylin and eosin. Inflammation was scored by a pathologist using an inflammation scale from – to + +, with – indicating no inflammation, + denoting mild inflammation predominantly infiltrated with neutrophils and ++ indicating active inflammation infiltrated with neutrophils and lymphocytes.

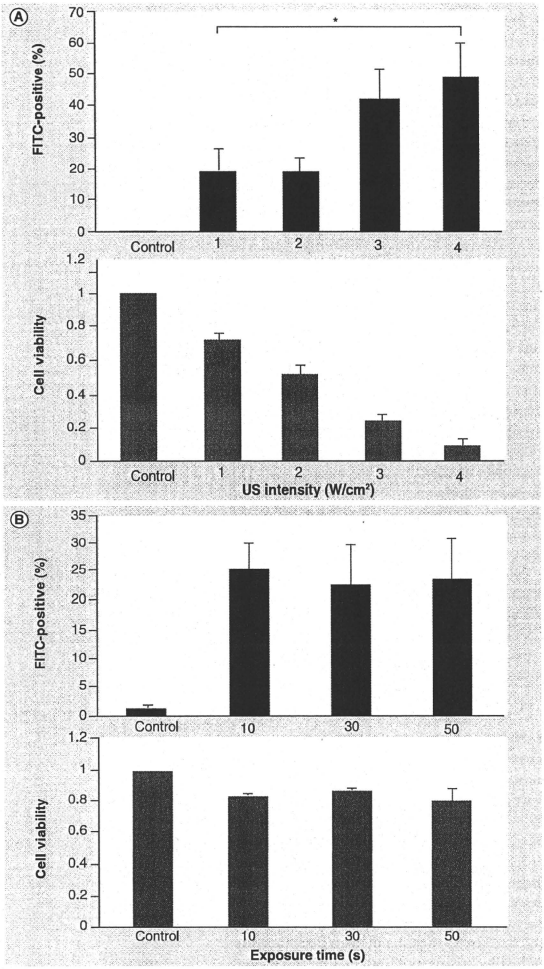

Figure 1. Determination of optimum ultrasound-mediated destruction of bubble liposome conditions. (A) Effects of US intensity on the rate of FITC-positive cells and cell viability in ultrasound-mediated destruction of bubble liposome (UBL). There was a significant difference in the rate of FITC-positive cells between 1–4 W/cm² intensities. **(B)** Effects of US exposure times on the rate of FITC-positive cells and cell viability in UBL. There were no significant differences in the rate of FITC-positive cells and cell viability between all groups.
*$p < 0.05$.
FITC: Fluorescein isothiocyanate; US: Ultrasound.

■ Statistical analysis

Statistical analysis was performed using Microsoft Excel (Microsoft Corporation, WA, USA). Values are expressed as mean ± standard deviation. Differences between groups were analyzed using two-sided Student's *t*-test. p-values lower than 0.05 were considered significant.

Results

■ Optimum conditions of UBL *in vitro*

US intensity

The effects of US intensity on FITC-positive cell rate and cell viability are shown in **Figure 1A**. The FITC-positive cell rates at 1, 2, 3 and 4 W/cm² US intensity were 19.71 ± 7.18% (mean ± SD), 19.91 ± 3.99, 42.52 ± 9.66 and 49.30 ± 11.55%, respectively. The rate of FITC-positive cells increased in an intensity-dependent manner. There was a significant difference in the FITC-positive cell rate between the UBL using 1 W/cm² US and that using 4 W/cm² US. The cell viabilities at 1, 2, 3 and 4 W/cm² US intensity were 70.40 ± 4.21, 50.42 ± 5.11, 22.76 ± 4.19 and 8.14 ± 3.22%, respectively. Conversely, cell viability decreased in an intensity-dependent manner.

■ US exposure time

The effects of US exposure time on FITC-positive cell rate and cell viability are shown in **Figure 1B**. The FITC-positive cell rates using 10, 30 and 50 s of US exposure time were 24.68 ± 5.14, 21.71 ± 7.72 and 22.98 ± 7.84%, respectively, with no significant difference between the three groups. The cell viabilities using 10, 30 and 50 s of US exposure time were 85.09 ± 2.02, 89.13 ± 1.31 and 82.81 ± 9.81, respectively.

■ BL concentration

The effects of BL concentration on FITC-positive cell rate and cell viability are shown in **Figure 2A**. The FITC-positive cell rates using 0.1, 0.2 and 0.3 mg/ml BL were 11.45 ± 4.04, 26.61 ± 5.72 and 19.54 ± 2.22%, respectively, with significant differences between 0.2 and 0.1 or 0.3 mg/ml. The cell viabilities using 0.1, 0.2 and 0.3 mg/ml BL were 90.24 ± 8.40, 72.32 ± 10.67 and 51.05 ± 12.09%, respectively.

■ Interval from BL addition to US exposure

The effects of interval from the BL addition to US exposure on FITC-positive cell rate and cell viability are shown in **Figure 2B**. The FITC-positive cell rates 15, 30, 60 and 300 s after the BL addition were 10.46 ± 0.03, 15.92 ± 3.05, 12.56 ± 2.40 and 5.27 ± 1.49%, respectively,

with significant differences between 30 and 15 or 300 s. The cell viabilities 15, 30, 60 and 300 s after the BL addition were 68.46 ± 10.78, 64.96 ± 2.81, 78.87 ± 8.27 and 89.28 ± 6.72%, respectively.

Taken together, the results show that the optimum conditions of BL are as follows: US intensity: 1 W/cm^2; US exposure time: 10 s; BL concentration: 0.2 mg/ml and interval: 30 s.

■ siRNA transfection using UBL at the optimum conditions determined by the simulation experiment *in vitro & in vivo*

At 24 h after treatment with UBL and luciferase siRNA, luciferase activity was not significantly suppressed compared with treatment with UBL and nonspecific siRNA (**Figure 3**). However, 48 h after treatment with UBL and luciferase siRNA, luciferase activity was significantly suppressed compared with treatment with UBL and nonspecific siRNA ($p = 0.036$; **Figure 3**).

The luciferase activities of the two groups increased with time (**Figure 4A**). The luciferase activity in the group treated with UBL and luciferase siRNA tended to be suppressed compared with that in the group treated with UBL and nonspecific siRNA up to 3 days after treatment (**Figure 4B**). However, there was no significant difference between both groups (**Figure 4B**).

■ Histological toxicity of UBL

Ultrasound-irradiated skin showed no recognizable changes in appearance (data not shown). Pathological changes in the skin following US exposure were not confirmed in mice treated with 0, 1 or 2 W/cm^2 US (**Figure 5**). Neutrophilic infiltration was, however, confirmed in mice treated with 3 or 4 W/cm^2 US (**Figure 5**; arrow).

Discussion & conclusion

This study mainly demonstrated the optimum conditions of UBL for siRNA transfection to the human bladder cell line RT-112^{Luc}. Gene or nucleic acid transfer utilizing UBL is expected to be a novel and promising strategy to overcome the severe adverse effects of intravesical administration of BCG currently used in clinics [2]. However, sonoporation has adverse effects according to the US energy and other conditions when it is used [28–30]. We therefore initially conducted several simulation experiments utilizing FITC-dextran transfer to cells as a surrogate marker to determine the best conditions of UBL with least toxic and maximum transfer effects. The molecular weight (MW) of FITC-dextran used in the present experiments

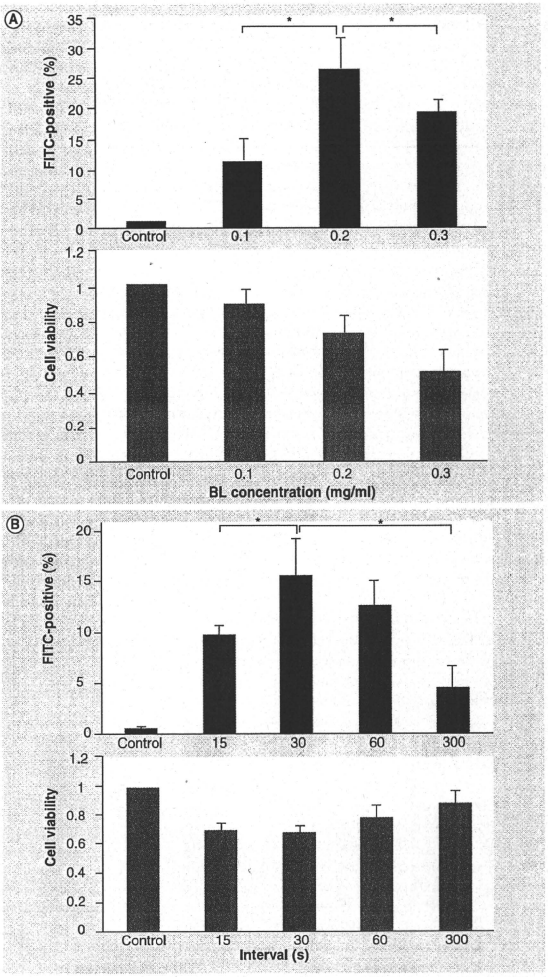

Figure 2. Determination of optimum ultrasound-mediated destruction of bubble liposome conditions. (A) Effects of bubble liposome (BL) concentration on the rate of FITC-positive cells and cell viability in ultrasound-mediated destruction of BL (UBL). There were significant differences in the rate of FITC-positive cells between 0.2 and 0.1 or 0.3 mg/ml. **(B)** Effects of intervals from BL addition to ultrasound exposure on the rate of FITC-positive cells and cell viability in UBL. There were significant differences in the rate of FITC-positive cells between 30 and 15 or 300 s. *$p < 0.05$.
FITC: Fluorescein isothiocyanate; BL: Bubble liposome.

was 10 kDa. Therefore, the pharmacodynamics of FITC-dextran according to the conditions of UBL may be extrapolated to that of siRNA, which has a MW of approximately 20 kDa.

Our preliminary study suggests that the BL should be used within 10 min after preparation, possibly due to its instability (data not shown). The optimum US intensity was further determined utilizing FITC-dextran transfer to cells. The ratio of FITC-positive cells increased but cell viability decreased in an intensity-dependent manner. These results indicate that higher gene transfer can be obtained by induction of microbubble collapse using higher US intensity, although such intensity was confirmed to cause cell toxicity. The optimum US intensity obtained *in vitro* appeared to be 1 W/cm^2 for siRNA transfer. These results are consistent with data published previously [17,18,31]. We also determined the optimum US exposure time by carrying out US irradiation to the cells for 10, 30 or 50 s. There were no significant differences in the rate of FITC-positive cells and cell viability in these three groups (**Figure 1B**). The present results were not in agreement with those of previous reports utilizing Optison™, wherein higher gene transfer was obtained with longer US exposure time [18,32]. Although the reason for these inconsistencies remain difficult to elucidate, it may be reasonable to conclude that a shorter US exposure time may be advantageous for US therapy in terms of exerting weaker adverse effects. In this study, the optimum US exposure time was determined to be 10 s. We also determined the optimum concentration of the BL for FITC-dextran transfer to cells. The ratio of FITC-positive cells in UBL with 0.2 mg/ml BL was the highest in the three groups. In addition, cell toxicity was higher when a higher concentration of the BL was used. These results are consistent with those of previous reports [20,32] and indicate a clear relationship between BL concentration and US effect. In this study, the optimum BL concentration was determined to be 0.2 mg/ml. Furthermore, we determined the optimum interval of the initiation of US exposure after the addition of the BL to the cell suspension. It was found that the optimum interval time was 30 s for the most effective FITC-dextran transfer to the cells. We speculated that the BL distributed throughout the solution 30 s after the addition of the BL and that the BL may be degraded afterward (**Figure 2B**). Taken together, several simulation experiments suggest the following optimum conditions of UBL: US intensity: 1 W/cm^2; US exposure time: 10 s; BL concentration: 0.2 mg/ml; interval: 30 s.

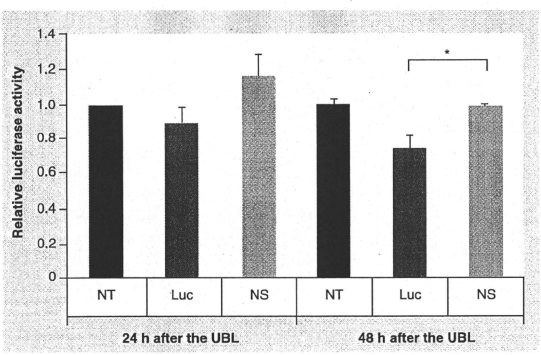

Figure 3. Suppression of luciferase activity by ultrasound-mediated destruction of bubble liposome with various siRNAs. Luciferase activity was affected by UBL with luciferase siRNA. There was a significant difference in the suppression of luciferase activity between UBL with luciferase siRNA and UBL with nonspecific siRNA 48 h after treatment.
*$p < 0.05$.
Luc: Luciferase siRNA; NS: Nonspecific siRNA; NT: Nontreatment; UBL: Ultrasound-mediated destruction of bubble liposome.

In addition, we found that UBL for luciferase siRNA transfer could suppress the expression of luciferase in RT-112^{Luc} cells (**Figure 3**). The results demonstrated that the optimal UBL conditions determined in this study could enable the transfer siRNA to cells.

The *in vivo* study demonstrated that within 48 h after UBL, luciferase activity with UBL for luciferase siRNA decreased compared with luciferase activity with UBL for nonspecific siRNA (**Figure 4**). However, this suppression disappeared 72 h after the treatment. This result is consistent with a previous report on sonoporation for the salivary gland, in which it was suggested that reduction of the RNAi effect was caused by siRNA degradation [15]. It was also previously suggested that the reduction of the RNAi effect in a dividing subcutaneous tumor might be caused by siRNA shortage due to tumor growth [3,33].

In the present study, UBL for siRNA transfer did not suppress luciferase activity significantly (**Figure 4B**). From the *in vivo* experiment, only a slight neutrophil infiltration as a result of inflammation was observed at 3 or 4 W/cm^2 US irradiation (**Figure 5**; arrow). Therefore, we speculate that higher US intensity may be used and this

achieves higher efficiency. Previous reports have demonstrated that sonoporation with higher US intensity mediates higher efficiency [14,17,31].

The present study demonstrated that the RNAi effect was reduced 3 days after UBL treatment (**FIGURE 4B**). Since the maximum effect of RNAi was confirmed 2 days after UBL in a previous study [15] and the present study (**FIGURE 4B**), serial UBL treatments after transurethral resection may contribute to continued gene suppression and adequate prevention of tumor recurrence. In practice, no severe adverse effects were observed when UBL treatment was administered three times for mouse skin (**FIGURE 5**). Therefore, multiple UBL treatments may be feasible for *in vivo* experiments as well as clinical use.

Another point of concern for the improvement of this method is to prevent naked siRNA from degradation by nuclease activity in the body. Since RNA is more degradable than DNA, siRNA may be degraded by nuclease in body fluids [34]. To protect siRNA from the degradation, chemical modifications such as cholesterol-modified siRNAs [35] or 2′-*O*-methyl-modified siRNAs [36] could be investigated.

Although an *in vivo* experiment with a subcutaneous tumor was conducted in the present study, UBL for siRNA transfer must be assessed in an orthotopic murine bladder tumor model [6,37]. In addition, for the future implication of UBL for siRNA transfer in the treatment of superficial bladder cancer, the target gene of this particular disease must be identified. When these areas have been addressed by UBL for siRNA transfer, UBL can be a novel, promising and powerful tool for the treatment of superficial bladder cancer.

Future perspective

In the future, optimal modification of US conditions or dose schedule for UBL may contribute to the suppression of the target gene in superficial bladder cancer. Furthermore, UBL may contribute to the prevention of recurrence of superficial bladder cancer.

Acknowledgements

The authors thank N Mie and M Ohtsu for technical assistance and K Shiina and K Abe for secretarial assistance.

Ethical conduct of research

The authors state that they have obtained appropriate institutional review board approval or have followed the principles outlined in the Declaration of Helsinki for all human or animal experimental investigations. In addition, for investigations involving human subjects, informed consent has been obtained from the participants involved.

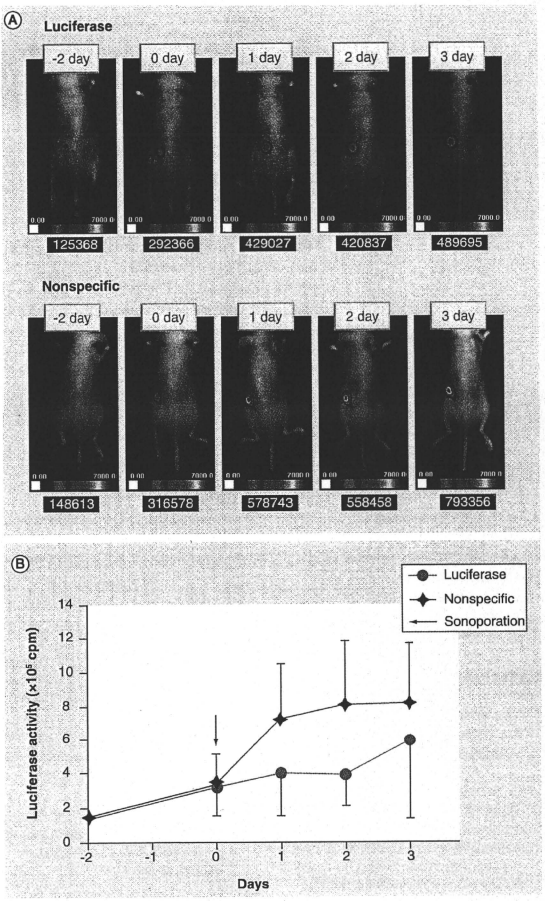

Figure 4. Suppression of luciferase activity by ultrasound-mediated destruction of bubble liposome for siRNA transfer in subcutaneous tumor model. (A) Mouse representing typical tendency in each group. Five images in all treatment groups indicate cpm -2, 0, 1, 2 or 3 days after ultrasound-mediated destruction of bubble liposome (UBL). **(B)** UBL with luciferase siRNA tended to suppress luciferase activity more than UBL with nonspecific siRNA *in vivo* (but not significant $p > 0.05$ 2 days after treatment).
cpm: Counts per minute.

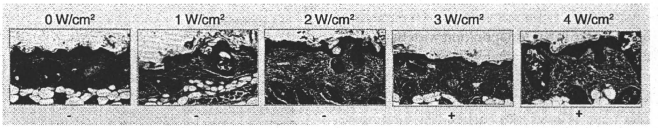

Figure 5. Adverse effects of ultrasound-mediated destruction of bubble liposome *in vivo*. Hematoxylin and eosin staining of skin (original magnification × 20). There were only slight infiltrations of neutrophils (arrow) at 3 or 4 W/cm² ultrasound exposure. Other adverse effects were not confirmed.

Financial & competing interests disclosure

This work was supported partly by a Grant-in-Aid from the 3rd Term Comprehensive Control Research for Cancer, Ministry of Health, Labor and Welfare (Yasuhiro Matsumura) and Scientific Research on Priority Areas from the Ministry of Education, Culture, Sports, Science and Technology (Yasuhiro Matsumura), and the Princess Takamatsu Cancer Research Fund (Yasuhiro Matsumura). The authors have no other relevant affiliations or financial involvement with any organization or entity with a financial interest in or financial conflict with the subject matter or materials discussed in the manuscript apart from those disclosed.

No writing assistance was utilized in the production of this manuscript.

Executive summary

- We initially conducted several simulation experiments utilizing fluorescein isothiocyanate (FITC)-dextran transfer to cells as a surrogate marker to determine the best conditions for ultrasound-mediated destruction of bubble liposome (UBL) with least toxic and maximum transfer effects.
- The ratio of FITC-positive cells increased in an intensity-dependent manner.
- The optimum conditions for UBL were determined as follows: ultrasound intensity: 1 W/cm²; US exposure time: 10 s; BL concentration: 0.2 mg/ml; interval: 30 s.
- The optimum UBL conditions determined in this study enabled siRNA transfer to cells.
- The *in vivo* study demonstrated that during the 48 h after UBL, luciferase activity with UBL for luciferase siRNA decreased compared with luciferase activity with UBL for nonspecific siRNA. However, this suppression disappeared 72 h after the treatment. UBL conditions must therefore be improved to obtain higher siRNA transfer.

Bibliography

Papers of special note have been highlighted as:
▪▪ of considerable interest

1 Gee J, Sabichi AL Grossman HB. Chemoprevention of superficial bladder cancer. *Crit. Rev. Oncol. Hematol.* 43(3), 277–286 (2002).

2 Shelley MD, Kynaston H, Court J *et al.* A systematic review of intravesical bacillus Calmette–Guerin plus transurethral resection vs transurethral resection alone in Ta and T1 bladder cancer. *BJU Int.* 88(3), 209–216 (2001).

3 Fire A, Xu S, Montgomery MK, Kostas SA, Driver SE, Mello CC. Potent and specific genetic interference by double-stranded RNA in *Caenorhabditis elegans*. *Nature* 391(6669), 806–811 (1998).

4 Elbashir SM, Harborth J, Lendeckel W, Yalcin A, Weber K, Tuschl T. Duplexes of 21-nucleotide RNAs mediate RNA interference in cultured mammalian cells. *Nature* 411(6836), 494–498 (2001).

5 Song E, Lee SK, Wang J *et al.* RNA interference targeting Fas protects mice from fulminant hepatitis. *Nat. Med.* 9(3), 347–351 (2003).

6 Nogawa M, Yuasa T, Kimura S *et al.* Intravesical administration of small interfering RNA targeting PLK-1 successfully prevents the growth of bladder cancer. *J. Clin. Invest.* 115(4), 978–985 (2005).

7 Ohta S, Suzuki K, Tachibana K, Yamada G. Microbubble-enhanced sonoporation: efficient gene transduction technique for chick embryos. *Genesis* 37(2), 91–101 (2003).

8 Ohta S, Suzuki K, Ogino Y *et al.* Gene transduction by sonoporation. *Dev. Growth. Differ.* 50(6), 517–520 (2008).

9 Michel MS, Erben P, Trojan L *et al.* Acoustic energy: a new transfection method for cancer of the prostate, cancer of the bladder and benign kidney cells. *Anticancer Res.* 24(4), 2303–2308 (2004).

10 Shohet RV, Chen S, Zhou YT *et al.* Echocardiographic destruction of albumin microbubbles directs gene delivery to the myocardium. *Circulation* 101(22), 2554–2556 (2000).

11 Sonoda S, Tachibana K, Uchino E *et al.* Gene transfer to corneal epithelium and keratocytes mediated by ultrasound with microbubbles. *Invest. Ophthalmol. Vis. Sci.* 47(2), 558–564 (2006).

12 Duvshani-Eshet M, Baruch L, Kesselman E, Shimoni E, Machluf M. Therapeutic ultrasound-mediated DNA to cell and nucleus: bioeffects revealed by confocal and atomic force microscopy. *Gene Ther.* 13(2), 163–172 (2006).

13 Tsunoda S, Mazda O, Oda Y *et al.* Sonoporation using microbubble BR14 promotes pDNA/siRNA transduction to murine heart. *Biochem. Biophys. Res. Commun.* 336(1), 118–127 (2005).

14 Saito M, Mazda O, Takahashi KA *et al.* Sonoporation mediated transduction of pDNA/siRNA into joint synovium *in vivo*. *J. Orthop. Res.* 25(10), 1308–1316 (2007).

▪▪ **Shows siRNA transfer to synovium by sonoporation *in vivo*. An effect of siRNA transfer to tissue by sonoporation *in vivo* was confirmed in this report.**

15 Sakai T, Kawaguchi M, Kosuge Y. siRNA-mediated gene silencing in the salivary gland using *in vivo* microbubble-enhanced sonoporation. *Oral. Dis.* 15(7), 505–511 (2009).

■■ **Shows siRNA transfer to salivary gland by sonoporation *in vivo*. It also refers to a period of siRNA-induced gene silencing by sonoporation.**

16 Suzuki J, Ogawa M, Takayama K *et al.*, Ultrasound-microbubble-mediated intercellular adhesion molecule-1 small interfering ribonucleic acid transfection attenuates neointimal formation after arterial injury in mice. *J. Am. Coll. Cardiol.* 55(9), 904–913.

17 Kinoshita M, Hynynen K. A novel method for the intracellular delivery of siRNA using microbubble-enhanced focused ultrasound. *Biochem. Biophys. Res. Commun.* 335(2), 393–399 (2005).

18 Kinoshita M, Hynynen K. Key factors that affect sonoporation efficiency in *in vitro* settings: the importance of standing wave in sonoporation. *Biochem. Biophys. Res. Commun.* 359(4), 860–865 (2007).

19 Newman CM, Bettinger T. Gene therapy progress and prospects: ultrasound for gene transfer. *Gene Ther.* 14(6), 465–475 (2007).

20 Li T, Tachibana K, Kuroki M. Gene transfer with echo-enhanced contrast agents: comparison between Albunex®, Optison™, and Levovist® in mice– initial results. *Radiology* 229(2), 423–428 (2003).

21 Taniyama Y, Tachibana K, Hiraoka K *et al.* Local delivery of plasmid DNA into rat carotid artery using ultrasound. *Circulation* 105(10), 1233–1239 (2002).

22 Suzuki R, Takizawa T, Negishi Y *et al.* Gene delivery by combination of novel liposomal bubbles with perfluoropropane and ultrasound. *J. Control. Release* 117(1), 130–136 (2007).

23 Suzuki R, Takizawa T, Negishi Y *et al.* Tumor specific ultrasound enhanced gene transfer *in vivo* with novel liposomal bubbles. *J. Control Release* 125(2), 137–144 (2008).

24 Suzuki R, Oda Y, Utoguchi N, Maruyama K. Progress in the development of ultrasound-mediated gene delivery systems utilizing nano- and microbubbles. DOI:10.1016/j.jconrel.2010.05.009 *J. Control Release* (2010) (Epub ahead of print).

25 Suzuki R, Namai E, Oda Y *et al.* Cancer gene therapy by IL-12 gene delivery using liposomal bubbles and tumoral ultrasound exposure. *J. Control Release* 142(2), 245–250 (2010).

26 Kodama T, Tomita N, Horie S *et al.* Morphological study of acoustic liposomes using transmission electron microscopy. *J. Electron Microsc. (Tokyo)* 59(3),187–196 (2010).

27 Negishi Y, Endo Y, Fukuyama T *et al.* Delivery of siRNA into the cytoplasm by liposomal bubbles and ultrasound. *J. Control Release* 132(2), 124–130 (2008).

28 Miller DL, Pislaru SV, Greenleaf JE. Sonoporation: mechanical DNA delivery by ultrasonic cavitation. *Somat. Cell Mol. Genet.* 27(1–6), 115–134 (2002).

29 Wei W, Zheng-zhong B, Yong-jie W, Qing-wu Z, Ya-lin M, Bioeffects of low-frequency ultrasonic gene delivery and safety on cell membrane permeability control. *J. Ultrasound Med.* 23(12), 1569–1582 (2004).

30 Koch S, Pohl P, Cobet U, Rainov NG. Ultrasound enhancement of liposome-mediated cell transfection is caused by cavitation effects. *Ultrasound Med. Biol.* 26(5), 897–903 (2000).

31 Li YS, Davidson E, Reid CN, McHale AP. Optimising ultrasound-mediated gene transfer (sonoporation) *in vitro* and prolonged expression of a transgene *in vivo*: potential applications for gene therapy of cancer. *Cancer Lett.* 273(1), 62–69 (2009).

32 Han YW, Ikegami A, Chung P, Zhang L, Deng CX. Sonoporation is an efficient tool for intracellular fluorescent dextran delivery and one-step double-crossover mutant construction in *Fusobacterium nucleatum*. *Appl. Environ. Microbiol.* 73(11), 3677–3683 (2007).

33 Bartlett DW, Davis ME. Insights into the kinetics of siRNA-mediated gene silencing from live-cell and live-animal bioluminescent imaging. *Nucleic Acids Res.* 34(1), 322–333 (2006).

34 Urban-Klein B, Werth S, Abuharbeid S, Czubayko F, Aigner A. RNAi-mediated gene-targeting through systemic application of polyethylenimine (PEI)-complexed siRNA *in vivo*. *Gene Ther.* 12(5), 461–466 (2005).

35 Soutschek J, Akinc A, Bramlage B *et al.* Therapeutic silencing of an endogenous gene by systemic administration of modified siRNAs. *Nature* 432(7014), 173–178 (2004).

36 Morrissey DV, Blanchard K, Shaw L *et al.* Activity of stabilized short interfering RNA in a mouse model of hepatitis B virus replication. *Hepatology* 41(6), 1349–1356 (2005).

37 Watanabe T, Shinohara N, Sazawa A *et al.* An improved intravesical model using human bladder cancer cell lines to optimize gene and other therapies. *Cancer Gene Ther.* 7(12), 1575–1580 (2000).

Advanced Drug Delivery Reviews 63 (2011) 184–192

Contents lists available at ScienceDirect

Advanced Drug Delivery Reviews

journal homepage: www.elsevier.com/locate/addr

Preclinical and clinical studies of NK012, an SN-38-incorporating polymeric micelles, which is designed based on EPR effect☆

Yasuhiro Matsumura *

Investigative Treatment Division, Research Center of Innovative Oncology, National Cancer Center Hospital East, 6-5-1, Kashiwanoha, Kashiwa, 277-8577, Japan

ARTICLE INFO

Article history:
Received 4 March 2010
Accepted 21 May 2010
Available online 31 May 2010

Keywords:
Drug delivery system
EPR effect
NK012
SN-38
Clinical trial

ABSTRACT

Polymeric micelles are ideally suited to exploit the EPR effect, and they have been used for the delivery of a range of anticancer drugs in preclinical and clinical studies.

NK012 is an SN-38-loaded polymeric micelle constructed in an aqueous milieu by the self-assembly of an amphiphilic block copolymer, PEG–PGlu(SN-38). The antitumor activity was evaluated in several orthotopic tumor models including glioma, renal cancer, stomach cancer, and pancreatic cancer. Two independent phase I clinical trials were conducted in Japan and the USA.

In the preclinical studies, it was demonstrated that NK012 exerted significantly more potent antitumor activity with no intestinal toxicity against various orthotopic human tumor xenografts than CPT-11. In clinical trials, predominant toxicity was neutropenia. Non-hematologic toxicity, especially diarrhea, was mostly Grade 1 or 2 during study treatments. Total 8 partial responses were obtained.

According to data of preclinical studies, NK012 showing enhanced distribution with prolonged SN-38 release may be ideal for cancer treatment because the antitumor activity of SN-38 is time dependent. Clinical studies showed that NK012 was well tolerated and had antitumor activity including partial responses and several occurrences of prolonged stable disease across a variety of advanced refractory cancers. Phase II studies are ongoing in patients with colorectal cancer in Japan and in patients with triple negative breast cancer and small cell lung cancer in the USA.

Contents

1. Preface

Irinotecan hydrochloride (CPT-11) is now approved for the treatment of various cancers including colorectal and lung cancers [1–4]. CPT-11 is a prodrug and is converted to SN-38, a biologically active metabolite of CPT-11, by carboxylesterases (CEs). SN-38 is an analog of the plant alkaloid camptothecin which targets DNA topoisomerase I. SN-38 exhibits up to 1000-fold more potent cytotoxic activity against various cancer cells in vitro than CPT-11 [5]. Although CPT-11 is converted to SN-38 in the liver and tumors, the metabolic conversion rate is less than 10% of the original volume of CPT-11 [6,7]. Moreover, the conversion of CPT-11 to SN-38 depends on the genetic inter-individual variability of CE activity [8]. Thus, further efficient use of SN-38 might be

☆ This review is part of the *Advanced Drug Delivery Reviews* theme issue on "EPR effect based drug design and clinical outlook for enhanced cancer chemotherapy".

* Tel.: +81 4 7134 6857; fax: +81 4 7134 6866.
E-mail address: yhmatsum@east.ncc.go.jp.

0169-409X/$ – see front matter © 2010 Elsevier B.V. All rights reserved.
doi:10.1016/j.addr.2010.05.008

Table 1
Example of other DDS of campto in oncolgy.

Name	Platform	Clinical stage
NKTR-102	PEG	Phase II
PEP02	Liposome	Phase II
CPX-1	Liposome	Phase II
IT-101	Cyclodextrin	Phase II
EZN-2208	Branch-PEG	Phase II
SN-2310	Vitamin E	Phase I
IHL-305	Liposome	Phase I

of great advantage and maybe attractive for cancer treatment. To date, many DDS of campto have been developed and some of them are now under clinical evaluation (Table 1). Polymeric micelle-based anticancer drugs were originally developed by Kataoka et al. in the late 1980s or early 1990s [9–11]. Polymeric micelles were expected to increase the accumulation of drugs in tumor tissues by utilizing the EPR effect [12]. Micelle system can also incorporate various kinds of drugs into their inner core with relatively high stability by chemical conjugation or physical entrapment. Also, the size of micelles can be controlled within the diameter range of 20 to 100 nm to ensure that they do not penetrate normal vessel walls. With this development, it is expected that the incidence of drug-induced side effects may be decreased owing to the reduced drug distribution in normal tissues. NK012 is an SN-38-loaded polymeric micelle constructed in an aqueous milieu by the self-assembly of an amphiphilic block copolymer, PEG–PGlu(SN-38) [13].

In this paper, preclinical and clinical studies of NK012 were reviewed.

2. Preparation of an SN-38 conjugated poly(ethylene glycol)–poly (glutamic acid) block copolymer [PEG–PGlu(SN-38)] for NK012 construction

PEG–PGlu(SN-38) was synthesized as follows: a poly(ethylene glycol)–poly(glutamic acid) block copolymer [PEG–PGlu] was prepared according to the technique reported previously [14,15]. SN-38 was covalently introduced into the poly(glutamic acid) [PGlu] segment by the condensation reaction between the carboxylic acid on PGlu and the phenol on SN-38 with 1,3-diisopropylcarbodiimide and N,N-dimethylaminopyridine at 26 °C. Consequently, the poly(glutamic acid) segment obtained sufficient hydrophobicity. Accordingly, NK012 was constructed with self-assembling PEG–PGlu(SN-38), amphiphilic block copolymers, in an aqueous milieu. NK012 was obtained as a freeze-dried formulation and contained ca. 20% (w/w) of SN-38 (Fig. 1). The mean particle size of NK012 is 20 nm in diameter with a relatively narrow range. The percentage released of SN-38 from NK012 in phosphate buffered saline at 37 °C were 57% and 74% at 24 h and 48 h, respectively, and that in 5% glucose solution at 37 °C were 1% and 3% at 24 h and 48 h, respectively. These results indicate that NK012 can release SN-38 under neutral condition even without the presence of a hydrolytic enzyme, and is stable in 5% glucose solution. In the formulation of NK012, SN-38 is bound to carboxyl group of hydrophobic chain of the block copolymer via ester bond and hydrolyzed to release SN-38. This ester bond may be cut gradually but efficiently at weak basic condition (PBS, pH 7.4) but very stable at weak acidic condition (5% glucose, pH 4.0). Consequently, it is suggested that NK012 is stable before administration and starts to release SN-38, the active component, inside a tumor following the accumulation of micelles into tumor tissue by utilizing the EPR effect.

3. Preclinical studies

3.1. Pancreatic cancer

Human pancreatic cancer is well known to have the worst prognosis [16]. At the time of diagnosis, the vast majority of the cancer extends beyond the pancreas. Direct invasion to nearby organs such as the stomach, duodenum, colon, spleen, and kidney is common. Distant metastasis to the liver and peritoneal dissemination are also common [17,18]. Gemcitabine is a first-line therapy for patients with advanced pancreatic cancer; however, only a response rate within 6–11% was

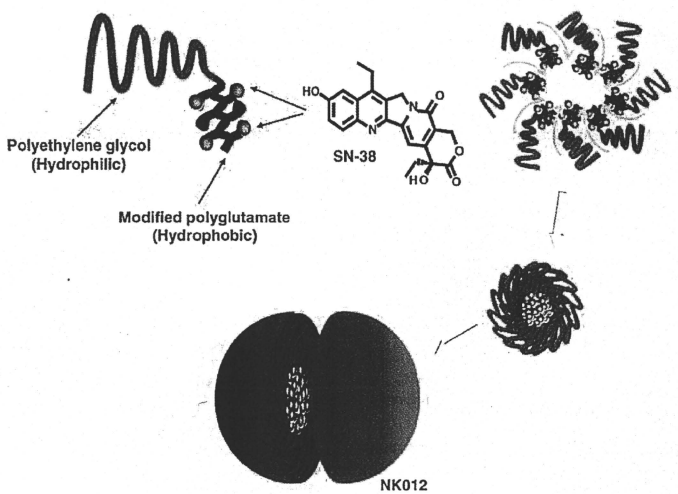

Fig. 1. Schematic structure of NK012. A polymeric micelle carrier of NK012 consists of a block copolymer of PEG (molecular weight of about Mw. 12,000 Da) and partially modified polyglutamate (about 20 units). Polyethylene glycol (hydrophilic) is believed to be the outer shell and SN-38 was incorporated into the inner core of the micelle.

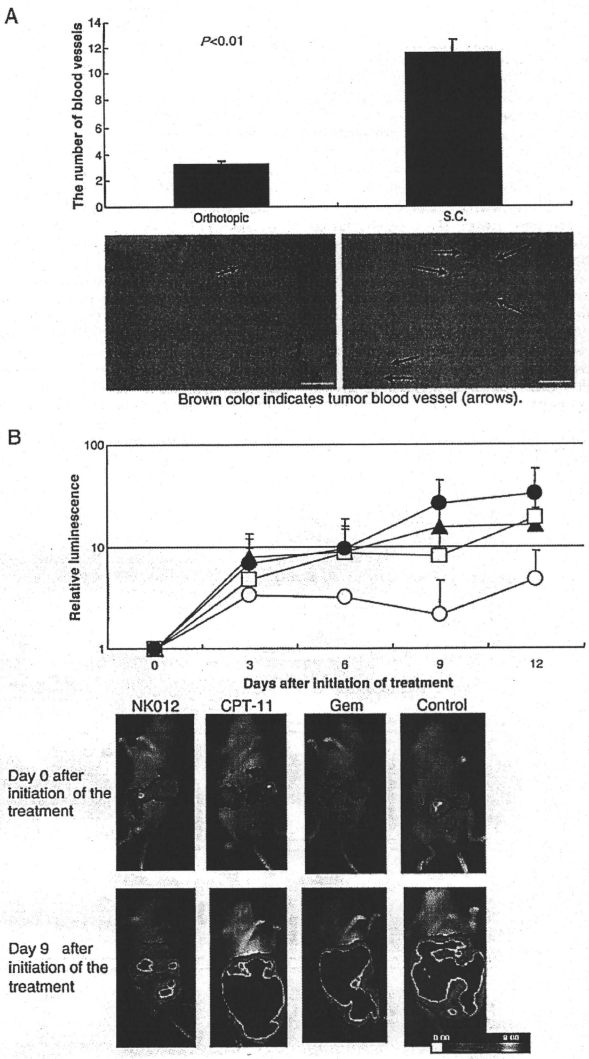

Fig. 2. (A) Number of blood vessels in orthotopic SUIT-2 tumor xenografts and subcutaneous (S.C.) tumor xenografts. After immunostaining with anti-factor VIII antibody, the number of tumor blood vessels (arrows) in each xenograft was counted. Column, mean + SD. $P<0.01$ (orthotopic vs S.C.). Scale bar: 200 μm. (B) Antitumor effects of NK012 in orthotopic tumor xenografts. Mice bearing SUIT-2 tumors were assigned into 4 groups 21 days after tumor inoculation. Mice were intravenously administered with NK012 (○) (30 mg/kg/day), CPT-11 (▲) (66.7 mg/kg/day), and 0.9% NaCl solution (●) (as a control) on days 0 (21 days after tumor inoculation), 4, and 8. Gemcitabine (□) (16.5 mg/kg/day) was administrated intraperitoneally on days 0, 3, 6, and 9. Representative luminescence intensity images obtained in individual control and treatment group mice on days 0 and 9. Points, mean + SD. $P=0.0074$ (NK012 vs control), $P=0.0231$ (NK012 vs CPT-11), $P=0.0239$ (NK012 vs gemcitabine).

observed in pancreatic cancer patients treated with gemcitabine [19,20]. The recent success of molecular-targeting agents has some impact on pancreatic cancer treatment. A recent phase III trial of gemcitabine alone vs gemcitabine and erlotinib (a tyrosine kinase inhibitor) in patients with advanced pancreatic cancer showed that overall survival was significantly improved with gemcitabine and erlotinib compared with gemcitabine and placebo. However, the improvement in median overall survival with gemcitabine and erlotinib was modest (6.24 months vs 5.91 months) [21]. Therefore, novel therapeutic approaches against invasive advanced pancreatic cancer are urgently needed. There are several reasons why pancreatic cancer is intractable clinically. One is that anticancer drugs are not efficiently and sufficiently delivered to the cancer cells within pancreatic cancer tissues. This is because human pancreatic cancer is hypovascular [22,23] and is rich in interstitial tissue, which may hinder efficient distribution of anticancer drugs to the entire pancreatic cancer tissue. We used an orthotopic pancreatic tumor model to evaluate the antitumor effects of NK012 because the orthotopic pancreatic cancer xenografts showed poorer vasculature and more abundant interstitium than the subcutaneous tumor xenografts (Fig. 2A). Moreover, peritoneal dissemination accompanied the orthotopic tumor. We have shown that NK012 has potent antitumor effects against orthotopic pancreatic tumors compared with gemcitabine and CPT-11, and that NK012 decreased the number of metastatic nodules in the peritoneal cavity (Fig. 2B). Thus, we admonish that it is better to use orthotopic tumor xenografts to evaluate antitumor activity against cancer characterized by few tumor vessels and high amount of tumor stroma. Moreover, enhanced accumulation, distribution, and retention of polymeric micelle-based anticancer drugs within the tumor tissue and the sustained release of anticancer drugs from the micelles are key elements for the treatment of hypovascular tumors [24].

3.2. Lung cancer

The median survival of small cell lung cancer (SCLC) patients treated with the CPT-11/cisplatin (cis-dichlorodiammineplatinum (II): CDDP) combination was significantly longer than that of SCLC patients treated with the etoposide/CDDP combination in a randomized phase III study conducted by the Japanese Cooperative Oncology Group (JCOG) [25]. Therefore, CPT-11/CDDP is considered to be one of the most active regimens against SCLC in Japan. One of the major clinically important toxic effects or dose limiting factors of CPT-11 is severe late-onset diarrhea [26]. We previously demonstrated that there was no significant difference in the kinetic character of free SN-38 in the small intestine of mice bearing the SCLC cell line SBC-3 and treated with NK012 and CPT-11 [13]. In this context, we investigated the advantages of NK012/CDDP over CPT-11/CDDP in mice bearing a SCLC xenograft in terms of antitumor activity and toxic effects, particularly intestinal toxicity. A significant difference in the relative tumor volume on day 30 was found between NK012/CDDP and CPT-11/CDDP treatments. Inflammatory changes in the small intestinal mucosa were rare in all NK012-treated mice, but were commonly observed in CPT-11-treated mice (Fig. 3). Moreover, a large amount of CPT-11 was excreted into the feces and high CPT-11

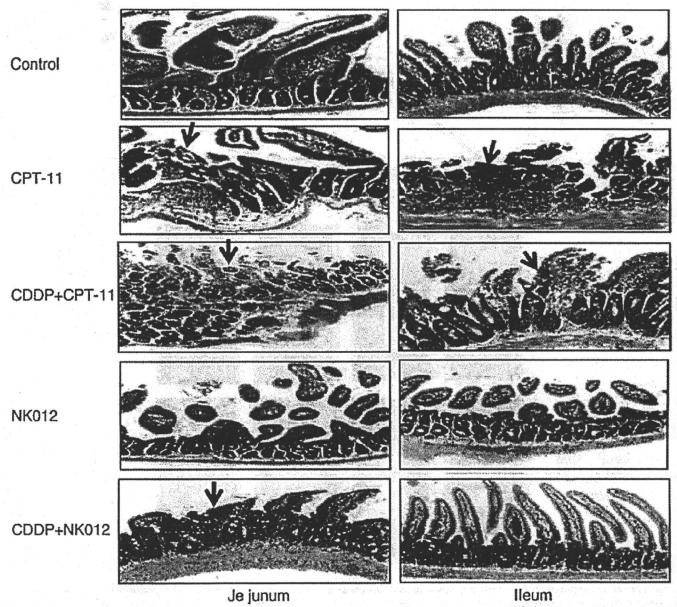

Fig. 3. Pathological findings and characteristic mucosal changes (arrows) in mouse. CPT-11 treatment group: healed erosion with fibrotic changes and lymphocytic invasion in the jejuna mucosa. Severe glandular arrangement. Active inflammation with inflammatory cell invasion and disappearance of gland ducts on the ileal mucosa. CPT-11/CDDP treatment group: healed erosion with scar-like fibrotic growth in the jejuna mucosa and mild inflammatory cell invasion into the ileal mucosa. NK012, NK012/CDDP treatment group and control: no inflammatory changes in the ileal mucosa. Mild shortening and decreased number of villi or mild inflammatory cell invasion in the jejuna mucosa in the NK012/CDDP treatment group.